The Selection and performance of Diamond Radiators used in Coherent Bremsstrahlung Experiments

J.D. Kellie [a] P.J.M. Clive [a] G.L. Yang [a] R. Beck [i] C. Gordon [a] C. Hall [e] J. W. Harris [b] R.T.Jones [f] D.Laundy [h] K. Livingston [a] I.J.D. MacGregor [a] J.C. McGeorge [a] J. Melone [a] A. Schmidt [i] P.A. Slaven [d] R.M. Vrcelj [c] D. Watts [g]

[a] *Dept. of Physics and Astronomy, University of Glasgow, Glasgow, Scotland*

[b] *Division of Earth Sciences, University of Glasgow, Glasgow, Scotland*

[c] *Pfizer Institute for Pharmaceutical Material Science, University of Cambridge, England*

[d] *University of Strathclyde, Glasgow, Scotland*

[e] *Element 6, The Netherlands*

[f] *University of Connecticut, Storrs, CT, USA*

[g] *Dept. of Physics, University of Edinburgh, Edinburgh, Scotland*

[h] *Daresbury Laboratory, Warrington, England*

[i] *Institut für Kernphysik der Universität Mainz, Germany*

Abstract

The bremsstrahlung emitted as a result of scattering electrons in thin diamond crystals provides a useful source of high energy photons for use in photonuclear experiments, since the coherent bremsstrahlung produced is linearly polarized. Techniques for selecting the most favourable diamonds have been investigated. These are optical polaroid analysis, X-ray topography and rocking curve measurements. The diamonds are characterised with a view to determining their performance as radiators, and bremsstrahlung spectra from a diamond radiator used at the Mainz MAMI-B facility are presented. The changes caused by high energy electrons to the crystal properties of the diamond and to the resulting coherent bremsstrahlung spectra are discussed.

Key words: Bremsstrahlung; Diamonds; Coherent Bremsstrahlung; Photonuclear studies

1 Introduction

A well established method for creating a beam of high energy linearly polarised photons for use in photonuclear studies is coherent bremsstrahlung production (1). The primary electron beam is scattered in a crystal whose regular lattice of atoms allows the recoil momentum to be taken up by the crystal as a whole, rather than by individual atoms. This occurs when the crystal is set at an angle to the incident electron beam such that the recoil momentum is equal to one of the crystal reciprocal lattice vectors, in a manner analogous to Bragg scattering.

In comparison to an incoherent bremsstrahlung spectrum from an amorphous radiator, a coherent bremsstrahlung spectrum has additional structure. Typical measured and calculated coherent and incoherent bremsstrahlung spectra are compared in figure 1. The solid black curves show the total measured photon energy spectra from nickel (top) and diamond (bottom). The dashed curves show theoretical fits to the data. (2). Figure 2 shows the total photon spectrum from a diamond divided by the spectrum from an amorphous radiator for the same electron beam energy. i.e. the relative intensity. The theoretical fit is shown as a dashed curve. For both figures 1 and 2 the fits are very good since it is difficult to distinguish them from the data points over most of the photon energy range. The strongest peak in the spectrum in figure 2 (at $\sim$330 MeV) arises from the (220) crystal planes and the sharp decrease in intensity at the upper side of this peak will be referred to as the 'coherent edge'. The spectrum in figure 2 is normalized to have a value of 1 at the minimum of the edge. The structures at higher energy are due to the scattering from different crystal planes.

The main advantage of coherent bremsstrahlung is that the photons are linearly polarised. For example in the photon energy region where the intensity enhancement is greatest, the degree of linear polarisation can exceed 80% if the photon beam is suitably collimated. Diamond is particularly suitable as a radiator due to its high Debye temperature, which means that the amplitude of the thermal motion of the atoms in the lattice is small and the lattice structure is relatively unaffected by thermal effects. (3; 4).

Since diamond specimens always suffer from imperfections, one of the aims of the present study has been to find the extent to which they can be tolerated in coherent bremsstrahlung experiments. This can then be used as the basis for selecting suitable specimens. Ideally, the assessment technique should be simple and inexpensive but provide sufficient information to determine how well the diamond will perform as a radiator.

Diamonds are classified into four types, referred to as Ia, Ib, IIa and IIb (5). Type I have concentrations of nitrogen impurity varying from around 1 ppm. to greater than 10^3 ppm. The nitrogen in type Ia occurs in aggregated form, that is, the nitrogen atoms occur in the lattice in pairs, groups of four, or as part of other complexes formed with vacancies. In type Ib the nitrogen atoms

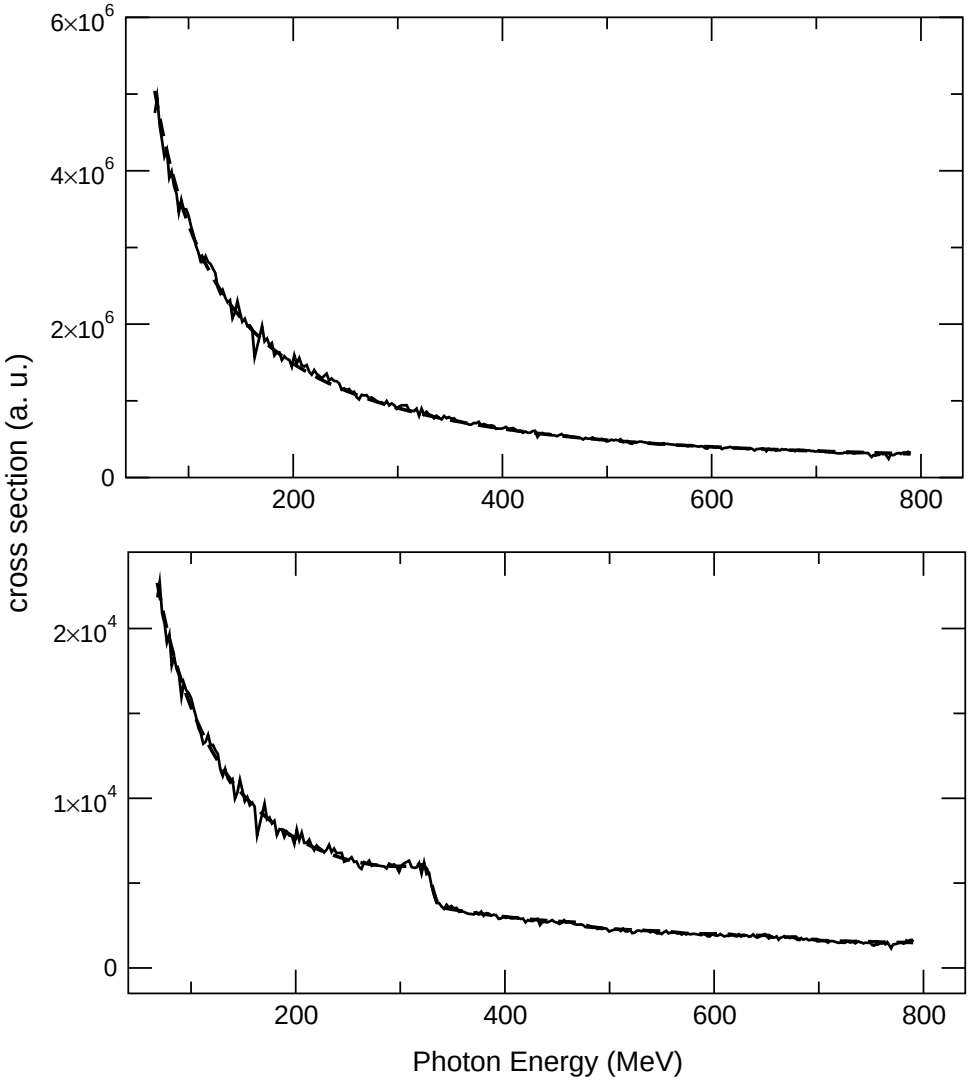

Fig. 1. Comparison of measured data (black line) and the theoretical least squares fit (dashed line) for the bremsstrahlung intensity for nickel (top) and diamond (bottom)

are substitutional and dispersed evenly through the volume of the diamond. Type II diamonds contain much less nitrogen than type I, in general less than 1 *ppm*. For natural diamonds, type II specimens are most probably the result of slow diamond growth. In the present paper both natural and synthetic industrial diamonds are assessed.

When an electron beam passes through a diamond radiator there is a spread in the direction of the electrons with respect to the crystal orientation due to three main causes; the divergence of the primary electron beam, multiple scattering of the electrons in the diamond and finally the variation in the crystal lattice arising from crystal defects. This angular variation degrades the coherent spectrum and it should be kept smaller than the bremsstrahlung

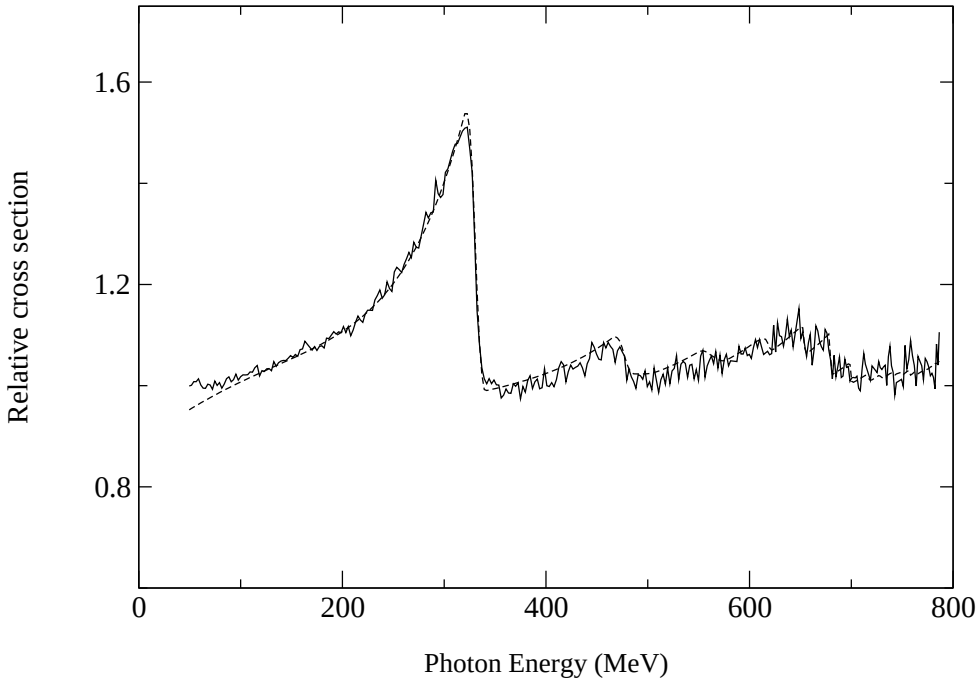

Fig. 2. Relative bremsstrahlung spectrum

characteristic opening angle,

$$\theta_{br} = \frac{mc^2}{E_0}$$

where m is the electron mass and E_0 the incident electron beam energy.
Since the present paper presents coherent bremsstrahlung spectra measured using the Glasgow tagged photon spectrometer (6; 7) at the 855 MeV electron accelerator in Mainz, we shall concentrate on coherent bremsstahlung production at 855 MeV. We shall also discuss the production at 12 GeV since this will be relevant for the planned new experiment GlueX at the Jefferson Laboratory (8) which will use linearly polarized photons from coherent bremsstrahlung with a 12 GeV beam.
A change in the orientation of the diamond with respect to the incident electron beam causes the coherent edge to shift. Figure 3 shows the calculated magnitude (1) of the shift for the coherent peak produced by the 220 reciprocal lattice vector for E_0 =855 MeV and E_0 =12 GeV for a range of values of $k = E_\gamma/E_0$ where E_γ is the bremsstrahlung photon energy. Indicated by the dashed lines are the shifts for E_γ ∼240 MeV, which is the coherent edge energy for measurements at Mainz which are discussed later in this paper, and for E_γ=8 GeV, which will be a typical energy for investigating the production of exotic hybrid mesons at GlueX (8). From figure 3 we find a change of magnitude of θ_{br} in the electron direction causes the energy of the coherent edge produced by the 220 reciprocal lattice vector to change by $\sim 2\%$ and $\sim 0.4\%$ of E_0 for the energies $E_\gamma = 240$ MeV and 8 GeV discussed above. It follows that

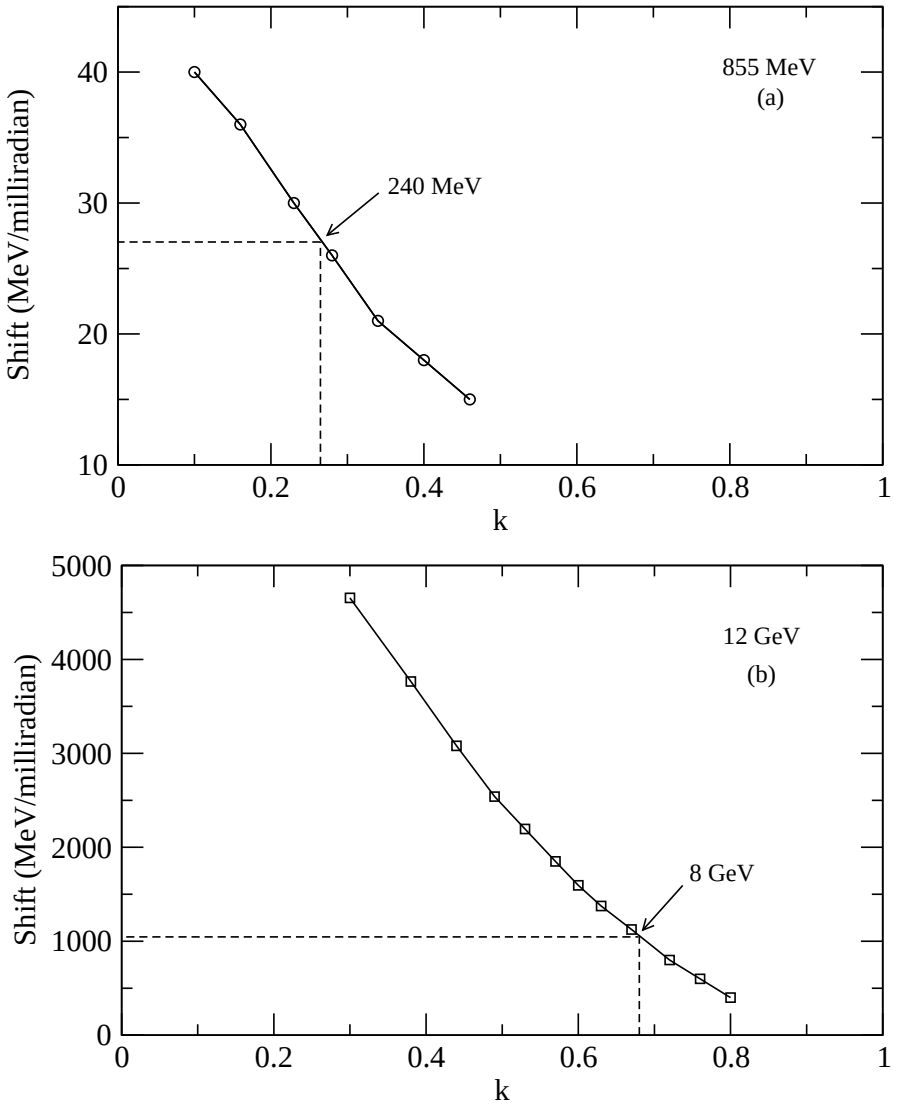

Fig. 3. Shift in position of the coherent edge from the 220 reciprocal lattice vector with respect to diamond orientation($Mev/milliradian$) for beam energies of 855 MeV and 12 GeV as a function of $k = \frac{E_\gamma}{E_0}$.

an electron angular distribution of this magnitude will broaden the structure of the coherent peak and reduce the maximum polarization (8). The values of θ_{br} for the Mainz and Jefferson Laboratory accelerators are around 600 μrad and 40 μrad respectively. Since the average divergence of the electron beam at Mainz is around 40 μrad (9) and at the Jefferson Laboratory will be around 12 μrad (8), the effect of beam divergence on the coherent bremsstrahlung spectra is or will be small for both laboratories.
Considering the spatial distribution of electrons undergoing multiple scattering, a reasonable approximation for the r.m.s. electron multiple scattering

angle is given by(10):

$$\theta_{sc} = \frac{19.2}{E_0}\sqrt{t} \times (1 + 0.038\ln(t))$$

where E_0 is expressed in MeV and t is the radiator thickness in radiation lengths (The radiation length is the distance for which the incident electron energy falls by a factor of e). We find, the ratio:

$$\frac{\theta_{sc}}{\theta_{br}} = \frac{19.2}{mc^2}\sqrt{t} \times (1 + 0.038\ln(t))$$

is independent of E_0, and hence a radiator of a given thickness will provide coherent bremsstrahlung spectra for which the effects of multiple scattering are equivalent at different beam energies. A reasonable upper limit for which the spreading of the coherent peak and the reduction in the polarization are small, is

$$\theta_{sc} = \frac{\theta_{br}}{2}.$$

This requires a diamond of thickness $\sim 40\ \mu m$, which is 3.6×10^{-4} radiation lengths.
The final point affecting the spread in the direction of the electrons with respect to crystal orientation depends on the occurrence of crystal defects. This is addressed by trying to obtain specimens which ideally would be diamond monocrystals. Section 2 describes the techniques used to identify specimens with highly regular lattices.

2 Apparatus and Methods

The samples discussed in this paper were chosen to illustrate some of the common features found in diamond wafers and also to compare different types of diamond. The samples have thicknesses between 50 and 120 μm. The details are given in table 1.
In characterising the diamonds to determine criteria for selecting the most suitable specimens to use as radiators in coherent bremsstrahlung experiments, three techniques have been used. The first is optical polaroid analysis in which the diamonds are illuminated from below using polarised light, and then viewed from above either directly or through another polaroid, crossed perpendicular to the polaroid below, such that only areas where local birefringence in the crystal caused by strain fields associated with defects can be

List of Diamond Specimens Investigated					
Sample	*Type*	*Thickness* (μm)	*Thickness* (*rad. lengths*)	*Plane*	*Synthetic/ Natural*
1	Ib	100	8×10^{-4}	(001)	Synthetic
2	Ib	50	4×10^{-4}	(001)	Synthetic
3	Ib	120	10×10^{-4}	(011)	Synthetic
4	Ib	110	9×10^{-4}	(001)	Synthetic
5	IIa	50	4×10^{-4}	(001)	Natural
6	Ib	100	8×10^{-4}	(001)	Synthetic

Table 1
A listing of the samples used in this survey.

seen.

The second and third techniques allow the defects to be studied with better resolution using X-rays. The X-rays wavelengths we used were 1 $\mathring{A}$ and 1.3 $\mathring{A}$. The first of these is X-ray topography in which an image of the sample is obtained from a diffracted parallel beam of X-rays. Defects and dislocations interrupt the perfect crystalline lattice and show up as contrast in the image. The second of these techniques is rocking curve measurements in which the test crystal is illuminated by a monochromatic X-ray beam and the diffracted intensity is measured as the test crystal is rotated around the Bragg angle corresponding to diffraction from a set of lattice planes. When diffracting from a perfect crystal, the rocking curve is not infinitely sharp but has a finite but small width. In reflection geometry, the rocking curve is given by a Darwin curve (11; 12). Deviations from a perfect crystal lattice, whether from defects and dislocations or from bending of the lattice and variation in lattice parameter, result in the rocking curve becoming broader than the theoretical value for a perfect crystal.

In the present paper, apart from a series of rocking curves for a sample which has suffered extensive damage from an 855 MeV electron beam, we present only transmission topographs and rocking curves for which the scattering planes in the diamond are at right angles to the surface of the diamond. The X-rays undergo photoelectric absorption in the diamond crystal but at around $1\mathring{A}$, the X-ray absorption depth is about 700 μm and therefore photoelectric absorption is not significant for our samples which have thicknesses of order 100 μm. This allowed us to make measurements in reflection and in transmission geometry. For reflection geometry, the penetration depth of the X-rays inside the Darwin curve into a perfect crystal is given by the extinction distance which is of order 10 microns in our case. Damage to the crystal however increases the X-ray penetration and we expect that with the radiation damaged specimens studied in reflection geometry, most of the diamond thick-

ness is sampled by the measurements. For transmission geometry, the X-rays sample the full thickness of the sample.
The rocking curve broadening may be interpreted in the mosaic model (13). In this model, an imperfect crystal is believed to be composed of a large number of small mosaic blocks; within each block the distribution of the atoms is perfect, but for different blocks, the crystal planes have different orientations. Usually it is assumed the mosaic angular distribution is Gaussian. The mosaic spread (σ_{mosaic}) is the square root of the variance of the orientation distribution. If it is assumed the rocking curve also has a Gaussian distribution, the mosaic spread can be estimated from the rocking curve width; ie the $F.W.H.M. = 2.35 \times \sigma_{mosaic}$. The measurement of rocking curve widths is the third technique adopted.
Although the X-rays are scattered by atomic electrons, whereas the electons in coherent bremsstrahlung are scattered by atomic nuclei, both processes are governed by the regularity of the lattice. Any deviations from this regularity, made apparent by the rocking curve width exceeding its theoretical value (see section 3), indicate the presence of crystal imperfections or regions of stress within the crystal.
In the present paper we examine whether there are any identifiable changes to the coherent bremsstrahlung spectrum from a diamond having a broadened rocking curve. In particular, a series of coherent bremsstrahlung spectra from a radiation damaged diamond which exhibits very large variations in rocking curve widths across the damaged region have been examined. The spectra were obtained at the MAMI-B Mainz microtron. The electron beam was passed through each crystal sample and the energies of the residual electrons measured using the Glasgow tagged photon spectrometer (6; 7). The photon energy spectrum was obtained directly from the residual electron energy spectrum. The diamond wafers were aligned relative to the electron beam according to the technique developed by Livingston (14).
The X-ray facility used was the synchrotron radiation source at Daresbury Laboratory, England. The experimental station lies at the end of an 80 m beam line ensuring that with adequate collimation the beam is effectively parallel. The topographs were obtained by exposing the whole area of the diamond samples to the main X-ray beam and recording the scattered intensity using photographic plates positioned at the Bragg angle. For the rocking curves, a double crystal diffractometer set-up was used. Collimated monochromatic X-rays from a silicon crystal monochromator in the main X-ray beam, were scattered from the diamond samples and detected using a NaI counter. A (+,-)configuration was adopted in which the scattering from the monochromator and the diamonds was in opposite directions.
Section 3 presents polarised light images, topographs and rocking curves as well as measurements of coherent bremsstrahlung spectra from a variety of diamond radiators.

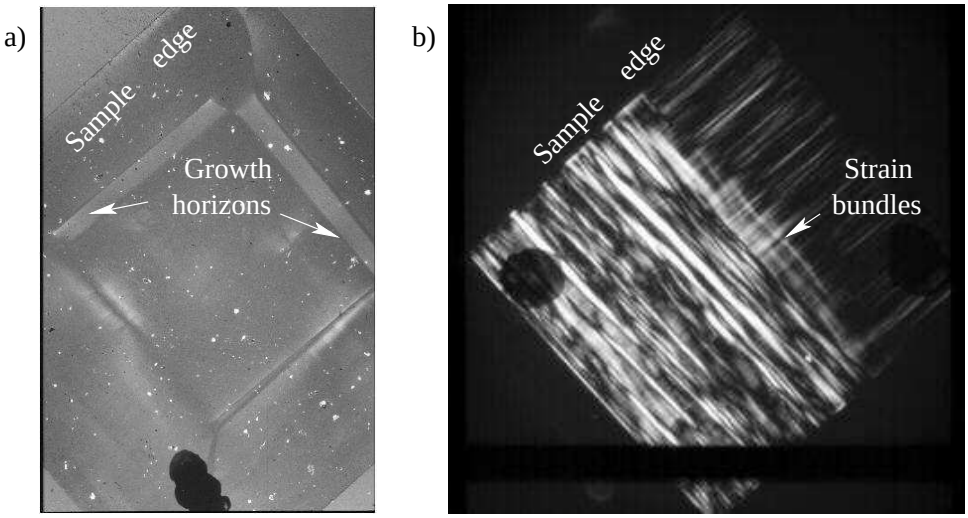

Fig. 4. Polarised light analyses of a) sample 1 and b) sample 5.

3 Results

Figure 4 shows the polarised light analyses of samples 1 and 5 and compares a synthetic type I with a natural type II. The black spots on figure 4(a) and 4(b) are identification marks. The black horizontal band at the bottom of 4(b) is an artifact of the photograph. Figure 4(a) shows an image of sample 1 taken with polarised light. It is virtually featureless, apart from some growth horizons, where strain has been induced due to differential growth rates on different families of crystal planes. There is also some dust on the surface of the diamond. Figure 4(b) shows an image of sample 5 taken with polaroids crossed at 90°. It shows bundles of linear features corresponding to line defects created as a result of the diamond undergoing plastic deformation in the Earth's upper mantle. The presence of these bundles of linear defects, sometimes referred to as a braided strain pattern, is typical of natural type II samples.

Figure 5 shows the transmission topographs and rocking curves of samples 1, 2 and 3, which are all type I industrial synthetic diamonds. The two vertical white lines on the topograph for sample 1 are due to the supporting wires for the sample. There is a clear similarity between the polarised light image and the topograph for sample 1. Due to its mounting, the light image is rotated by 45° with respect to the topograph but both show a central, approximately square, rather featureless region surrounded by growth horizons. Samples 1 and 2 are cut along (001) planes while sample 3 is cut along (011) planes - see table 1. All three samples were chosen to have central regions in their topographs which are more or less featureless. Two rocking curves are shown for sample 1. The rocking curve with the dashed line corresponds to the illumination of the entire crystal by the X-ray beam. All the other rocking curves shown correspond to the illumination of a central 0.25 mm square spot on the diamond. For samples 1 2, and 3 it is seen that a relatively featureless

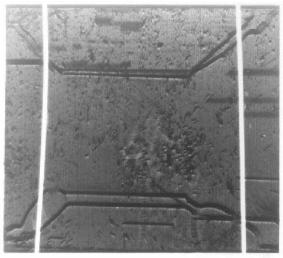

Sample 1

Transmission topograph

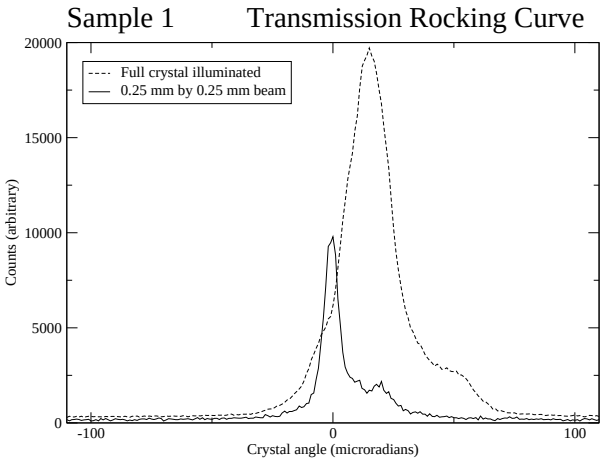

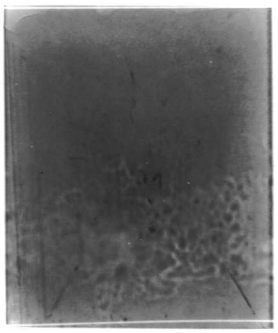

Sample 2

Transmission topograph

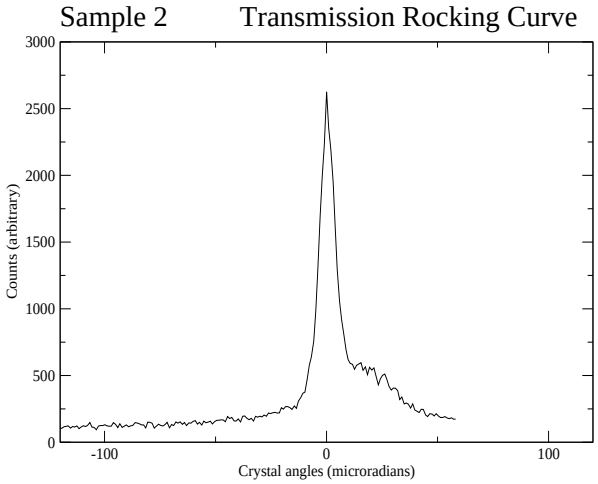

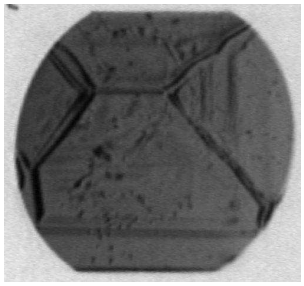

Sample 3

Transmission topograph

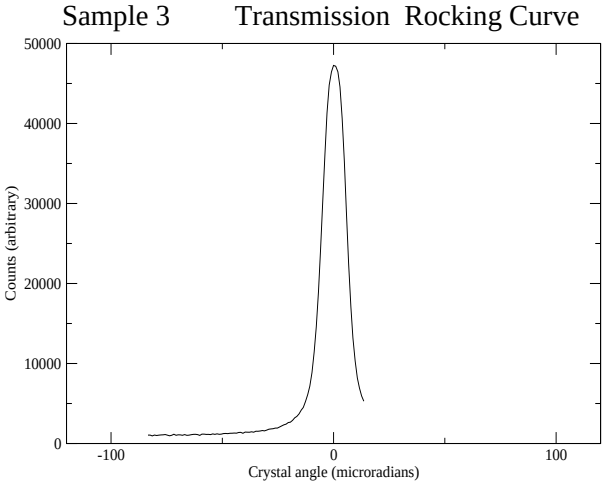

Fig. 5. Transmission topographs and rocking curves of samples 1, 2 and 3.

topograph correlates with a narrow rocking curve.

Figure 6 shows the topographs and rocking curves for samples 4 and 5. Sample 4 is a type I industrial synthetic whose topograph shows the imprint of the seed from which it was grown. It is seen that sample 5, a type II natural

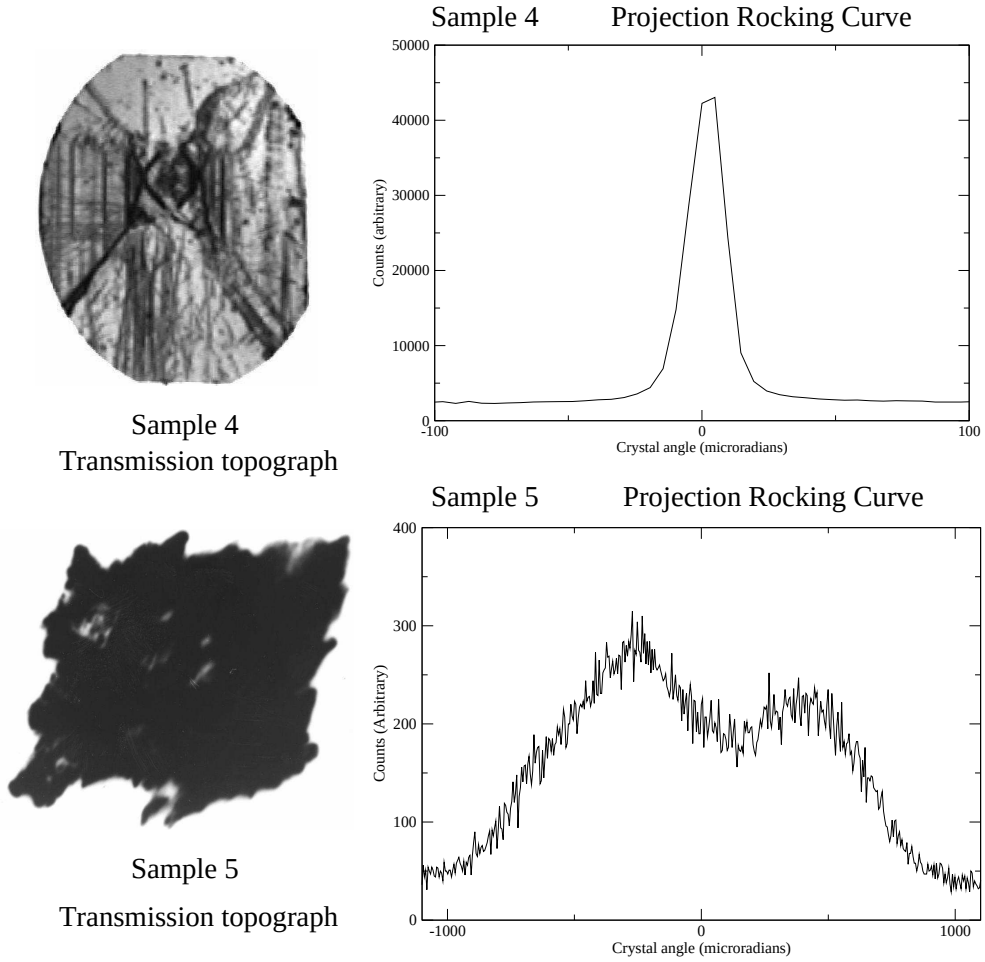

Fig. 6. Transmission topographs and rocking curves of samples 4 and 5.

diamond, which shows considerable evidence of strain in the polarized light analysis, has a very broad rocking curve, and its topograph is severly misshapen.

Table 2 summarises the rocking curve results from these samples. It also gives rocking curve data for a sixth sample for which coherent bremsstrahlung spectra were measured using the Glasgow tagger at Mainz. The F.W.H.M., W_{meas}, for the measured rocking curves can be compared with the theoretical F.W.H.M., W_{th}, for an ideal lattice as predicted by dynamical X-ray scattering theory (12). i.e.:

$$W_{th} = 2 \times (\frac{e^2}{m_e c^2}) \times \frac{\lambda^2 |F|}{\pi a^3 \sin 2\theta_B}$$

where λ is the X-ray wavelength, a is the lattice parameter for diamond, and θ_B is the Bragg scattering angle. $F_{hkl} = \alpha f_{hkl}$, where α is 8 or $4\sqrt{2}$ depending on the reflection and f_{hkl} is the atomic scattering factor for a carbon atom. The atomic planes used were (004) planes for samples 1,2,4,5 and 6 and (022)

Rocking Curves Widths							
Sample	*Type*	λ *(Å)*	*Plane*	θ_B	*Beamsize (mm×mm)*	W_{th} *(μrad)*	W_{meas} *(μrad)*
1	Ib	1	(004)	33°.9	0.25 × 0.25	5.4	6.7
2	Ib	1	(004)	33°.9	0.25 × 0.25	5.4	8.6
3	Ib	1.3	(022)	31°.1	0.25 × 0.25	11.9	12.4
4	Ib	1.3	(004)	47°.2	0.25 × 0.25	8.6	17.5
5	IIa	1	(004)	33°.9	0.25 × 0.25	5.4	∼ 1200
6	Ib	1	(004)	33°.9	0.25 × 0.25	5.4	30

Table 2
A table showing the rocking curve widths of the various samples.

planes for sample 3 - these being the lowest order allowed reflections. The X-ray wavelengths were chosen to make W_{th} less than 10 μrad for the (001) diamonds. For the (011) diamond W_{th} is slightly larger, having a value of ~ 12 μrad.
From the information presented in figures 5 and 6 and table 2, we can make the following observations:
a) The small X-ray spot on samples 1, 2 and 3 gives sharp structure which is not much larger than the theoretical value for a perfect crystal. It is reasonable to conclude the full widths of the distributions (which are in the range from 6.7 to 12.4 μrad) are related to the angular ranges of the microcrystal axes in the mosaics of the samples. It is noticeable for sample 1 that this angular range increases when the whole crystal is measured as would be expected.
b) The smooth rocking curve shape of sample 4 is consistent with this picture, but it has a more uniform range of crystal axis directions.
c) Sample 5 shows a wide range of crystal axis directions, but there is no direct evidence whether this is produced by many good quality microcrystals, or, as the strain pattern seen in the polarized light picture suggests, that deformation of the lattice is a more probable explanation.
So far we have discussed techniques for measuring how closely the lattice structure of a diamond which has not been exposed to a high energy electron beam matches that of a perfect crystal. Using sample 6 we now investigate the effect the incident electron beam has on a diamond radiator.

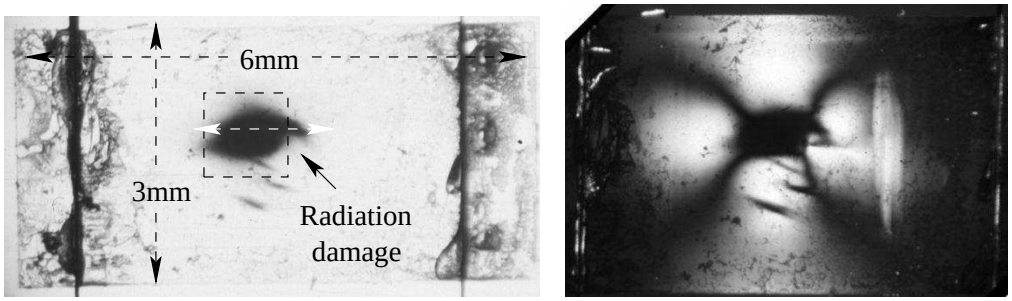

(a) (b)

Fig. 7. Petrographic microscopy of the radiation damaged diamond sample without (a) and with (b) crossed polaroids.

4 Effect of the incident electron beam.

Figure 7 shows optical polaroid images of sample 6, without 7(a) and with 7(b), crossed polaroids. Both images show regions of damage where the electron beam (around 10^{19} electrons in total) passed through the diamond. The dark vertical lines on the left and right of image (a) are supporting wires, and the dark areas around the wires are due to the glue holding the diamond to the wires changing colour after exposure to radiation.

The region of damage, which is outlined by the square box with dashed line edges in figure 7(a), was examined by measuring a set of reflection rocking curves along the white arrowed line in figure 7(a) at the Daresbury SRS with an X-ray beam collimated to a 0.25 mm square. In addition, coherent bremsstrahlung spectra were obtained for a series of points within the damaged region at the tagged photon facility in Mainz. The electron beam was focused to a spot approximately 0.1 mm in diameter.

The rocking curves are shown in figure 8. The rocking curves from the badly damaged region are much broader than those far from the damage centre. Far from the damage centre, the widths can probably be interpreted in terms of the mosaic model. However, in the damaged region, the mosaic model is probably too simplistic to provide a realistic description of the crystal lattice, and accordingly for the damaged region in sample 6 we use σ_{damage} rather than σ_{mosaic}. From the rocking curves, we estimate σ_{damage} is about 120 μrad - see section 5. Far from the damage center σ_{mosaic} is about 10 μrad. This indicates that away from the area which has been exposed to the electron beam, the diamond has a lattice structure which is almost perfect.

We now consider measured coherent bremsstrahlung spectra from the damaged region. Firstly we look for evidence that the damage could have changed the ratio of coherent to incoherent bremsstrahlung between the damaged and undamaged regions of the sample.

The bremsstrahlung from a crystal has a coherent part and an incoherent part. The incoherent part also contains a crystal contribution and an electron contribution. Using a computer programme developed by Natter (2) which calculates

the bremsstrahlung from both a diamond single crystal and an amorphous radiator, we find the best theoretical fit to an experimental bremsstrahlung spectrum from a diamond radiator by adding an adjustable extra incoherent component to the theoretical intensity and minimize X^2, where

$$X^2 = \sum_{spectra\ \ channels} (I_{me} - (\alpha I_{dt} + \beta I_{nt}))^2.$$

I_{me} is the measured intensity of diamond bremsstrahlung, I_{dt} is the calculated theoretical intensity of diamond bremsstrahlung, and I_{nt} is the calculated theoretical amorphous intensity. α and β are two parameters, which are varied to minimize X^2, and hence find the best fit. The incoherent contribution I_{nt} uses the theoretical approach of Hubbell (15).

The results of fitting the experimental bremsstrahlung spectra from sample

No.	1	2	3	4	5	6	7	8	9	10
x(mm)	-1.5	-1.2	-0.9	-0.6	-0.3	0	0.3	0.6	0.9	1.2
μ *(%)*	7.8	8.5	9.4	9.9	8.1	9.0	11	9.2	9.4	10
X^2	3.35	2.38	3.13	2.20	3.19	3.34	3.93	3.00	3.04	4.13

Table 3
Least squares simulation results; $\mu = \beta/\alpha$ and x is the position along the white arrowed line shown in figure 7(a). The damage centre is defined by x=0.

6 are summarized in table 3.

It is found that, after introducing the extra incoherent background, the fitted theoretical results agree well with the measured spectra. The amount of extra incoherent background is estimated by the parameter $\mu = \beta/\alpha$. The spectra were taken at different points along a line going through the radiation damaged region, where the $x = 0\ mm$ point is located at the damage center. The bottom row in table 3, lists the values of X^2 for different positions. The consistency of the values for X^2 demonstrates that the confidence level of the fits does not vary significantly across the damaged region. Although, in the damaged region, the beam electrons caused many defects, as can be observed from the discoloration around the damage center and from the wide rocking curve widths, there is no significant change in the amount of extra incoherent background required between the damaged and the undamaged regions. This means the disorder caused by the radiation at the dose level and electron beam energy used, has little effect on the relative magnitude of the incoherent bremsstrahlung spectrum. It is possible that the extra incoherent background indicated in table 3 is due to limitations in the theoretical description of the bremsstrahlung spectrum from diamond.

Another factor that affects the incoherent bremsstrahlung background is the radiator temperature (3). The background increases with temperature, and we find the extra background in table 3 can be accounted for by assuming

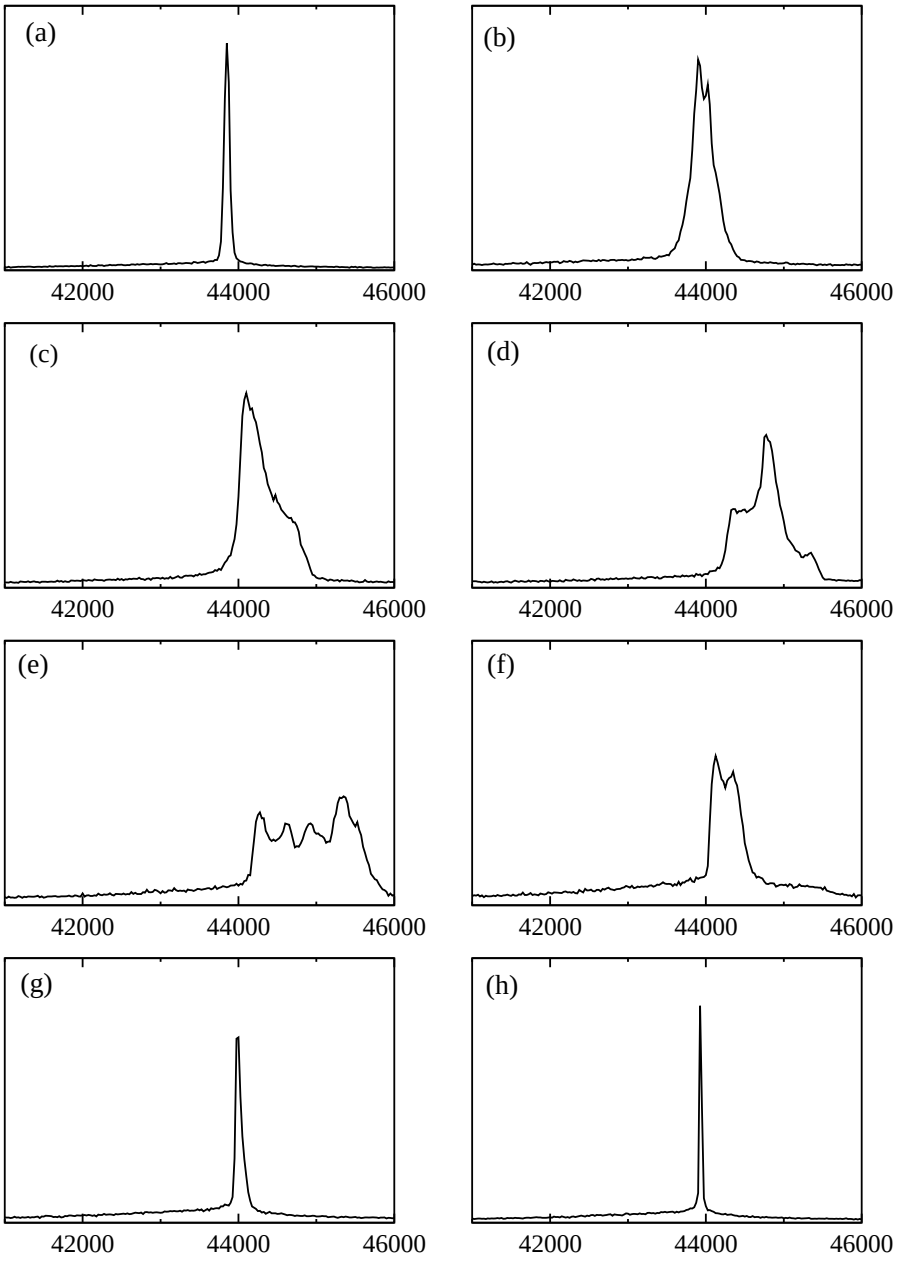

Fig. 8. Rocking curves at different positions along a line going through the radiation damaged center. For a-h, each point has a distance from the damage center of: -0.75mm, -0.50mm, -0.25mm, -0.0mm, 0.25mm, 0.50mm, 0.75mm, 1.0mm

the radiator temperature increases to about 800 K. At present, the diamond temperature can not be measured directly during the bremsstrahlung measurements, but it is possible to estimate an upper limit for the temperature. In our experiments, the diamond radiator is glued to two vertical tungsten wires by an organic glue. Since a temperature higher than 500 K will destroy the glue, and the diamond has never separated from the wires, the radiator

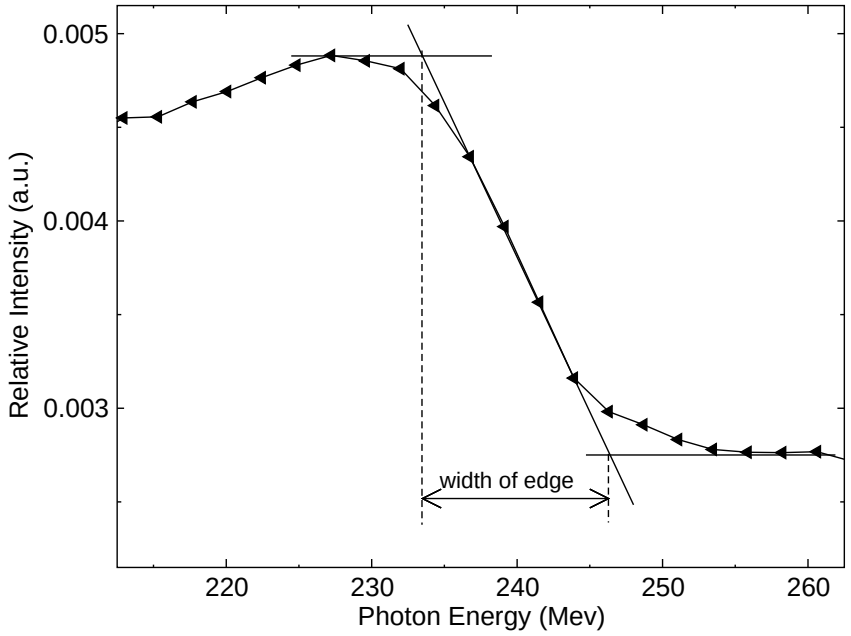

Fig. 9. Definition of the width of the coherent peak edge.

temperature is not very high. An estimate based on the rate at which energy from the electron beam is deposited in the diamond and the rate at which heat is radiated from it, suggests that the radiator temperature does not exceed 400 K in normal conditions(8). Hence, it is unlikely the radiator temperature influenced the incoherent part of the bremsstrahlung significantly.

Though crystal imperfections caused by the electron beam have little effect on the incoherent bremsstrahlung, we have observed some effects on the coherent part. We find that for the radiation damaged diamond (sample 6) and also a plastically deformed diamond, which is not described explicitly in the present paper, the width of the coherent edge becomes broader. The way we define the coherent edge width is illustrated in figure 9. The two straight lines parallel to the horizontal axis go through the maximum and minimum of the coherent edge, and the third line defining the slope of the edge intersects the two horizontal lines. These two intersections define a line segment, the projection of which onto the horizontal axis defines the width of the edge. Figure 10 shows the width of the edge for different positions within the damaged region - see figure 7(a). The points are defined by x and z co-ordinates where the x axis lies along the white arrowed line shown on figure 7(a) and the z axis is at right angles to the line. It is seen that in figures 10 (b) and (c), the width changes with x, and reaches a maximum at about x=-0.5 mm. However, in figures 10 (a) and (d), the width of the edge is almost constant. The x scans at z=0.25 mm and 0.5 mm go through the radiation damaged region, whereas the z=0 mm and 1 mm scans are outwith the damaged region.

Comparing the rocking curve width measurements with the bremsstrahlung spectra for the damaged region in sample 6 we find a large width corresponds to a broader coherent bremsstrahlung peak edge, which is consistent with the

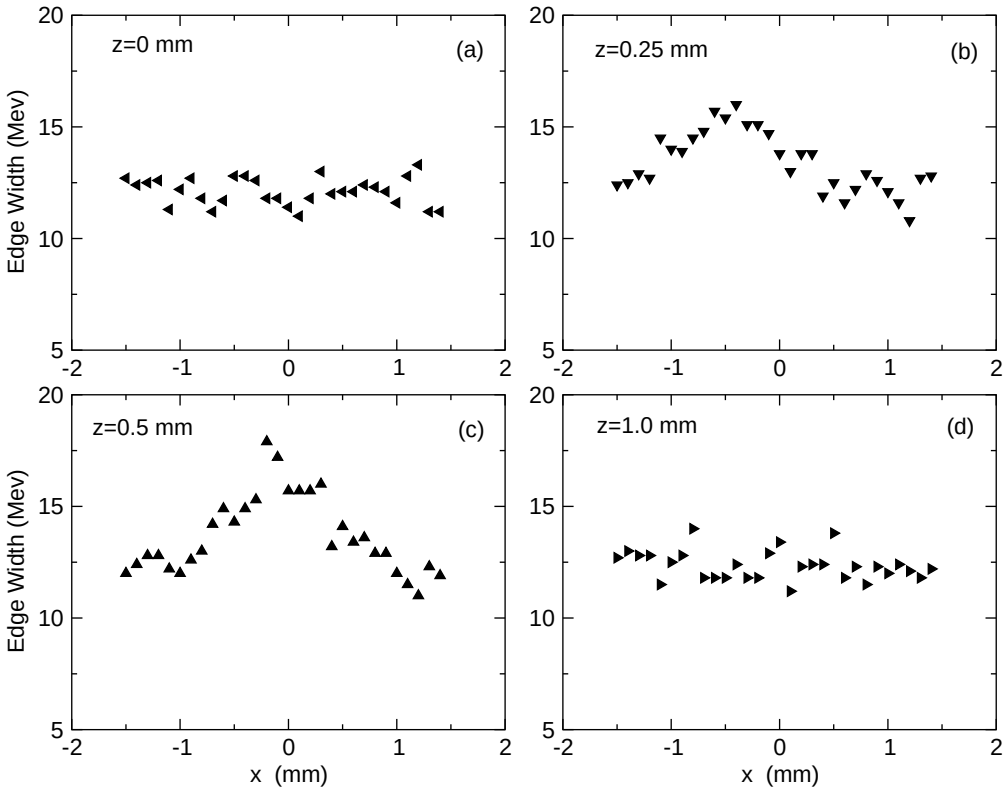

Fig. 10. The variation of the width of the coherent edge of sample 6 with x and z position. Referring to figure 7 the x-axis is horizontal and the z-axis vertical, with the origin at the damage center. When z=0.25mm and 0.5mm, the x scan goes through the damaged region.

prediction of Timm (3). By referring to figure 10, it appears that there is an underlying coherent edge width of around 12.5 MeV present across the whole of the diamond, but in the damaged region this increases to around 16 MeV.

5 Discussion.

Because mosaic spread, multiple scattering and beam divergence have similar effects on the diamond coherent bremsstrahlung spectrum, we should take them all into account. The total effective plane projected r.m.s. angular spread(σ_{total}) is given by

$$\sigma_{total}^2 = \sigma_{mosaic}^2 + \frac{1}{2}\sigma_{sc}^2 + \sigma_{beam}^2$$

where σ_{mosaic}, σ_{sc} and σ_{beam} refer to the mosaic spread, multiple scattering and beam divergence respectively. In the case of the damaged region in sam-

ple 6, σ_{damage} should replace σ_{mosaic}. (The plane projected multiple scattering formula is a factor of $\frac{1}{\sqrt{2}}$ less than the space formula which is given in section 1 (10)). We also take an average throughout the thickness of the diamond to describe the multiple scattering. This introduces the factor of 1/2 since multiple scattering varies predominantly as the square root of the thickness.
The diamond (sample 6) which was exposed to the 855 MeV electron beam at Mainz has a thickness of 100 μm and hence an average plane projected r.m.s. multiple scattering angle of about 235 μrad. The plane projected beam divergence was believed to be less than 100 μrad in our experiments(9), and for the present analysis we use a value of 50 μrad. From figure 8(e) at the center of the damaged region, the rocking curve seems to consist of at least 4 overlapping peaks each of which has a width comparable to the widths of the most prominent features in figures 8(b), (c), (d) and (f). Since the main X-ray beam at Daresbury is collimated to a 0.25 mm square and the Mainz electron beam has a diameter of 0.1 mm, the X-rays are able to sample the damage resulting from several closely spaced electron beam spots simultaneously. This could explain the shape of the rocking curve in figure 8(e). In the damaged region σ_{damage} is estimated as 120 μrad from the average width of the most prominent structures in the rocking curves associated with the damaged region. Away from the damage center σ_{mosaic} is about 10 μrad. Hence the total effective angular spread is about 270 μrad around the damage center and about 240 μrad away from the damaged region. Consequently, for the Mainz beam energy of 855 MeV and the 100 μm radiator used for the measurements, the overall angular spread does not change too significantly even although the rocking curve width shows such a large difference between the damaged and undamaged regions. This is due to the large multiple scattering contribution from the 100 μm thick diamond.
By referring back to figure 3(a), we can estimate the r.m.s. spread in the upper edge energy of the coherent peak at $E_\gamma \sim 240\ MeV$ from the angular changes of 240 μrad and 270 μrad. Values of around 6.5 and 7.3 MeV are found. To make a comparison with the results in figure 10, the coherent photon spectrum must be folded with the distribution of the edge energies. We find that the width W of the coherent edge is given by $W = (2.3 \pm 0.3)\sigma$ where σ is the r.m.s. spread in energies. Values for W of $15.0 \pm 2.0\ MeV$ and $16.8 \pm 2.2\ MeV$ are found for the undamaged and radiation damaged regions respectively. Although these are slightly larger than the coherent edge widths of $12.5 \pm 1.0\ MeV$ and $16.0 \pm 1.0\ MeV$ for the undamaged and damaged regions shown in figure 10, the agreement is sufficiently close to provide a qualitative explanation of the results shown in figure 10.
From figure 8, it also appears that the positions of the rocking curves change in a consistent way. ie: away from the damage centre, (a) and (h), the rocking curves have essentially the same position, but in moving towards the damage centre the curves shift towards the right, until at the center, (e), the left hand edge of the curves has moved by around 430 μrad. If we interpret this as

evidence that the orientation of the rocking curve scattering planes has been altered by this amount, the coherent edge of the bremsstrahlung spectrum would be shifted by around 12 MeV, which is not observed.
Another explanation of the effect, is that the radiation damage has produced a macro deformation throughout the volume of the crystal which has altered the inter-atomic plane spacing d. From the Bragg equation, d will change by a factor of $\sim 4 \times 10^{-4}$ if the scattering angle changes by $\sim$430 μrad. Furthermore , since the rocking curves for the damaged region have larger goniometer angles, the Bragg angle actually decreases and hence d increases slightly.
The reciprocal lattice vector will change by the same factor as d. Since the condition for coherent bremsstrahlung production is that the momentum transfer associated with the bremsstrahlung process equals the reciprocal lattice vector of the scattering planes, the coherent edge will shift. This is apparent from the equation linking the minimum longitudinal momentum transfer q_l to $k_C = \frac{E_\gamma{}^{edge}}{E_0}$ the fractional photon energy of the coherent edge. ie: $q_l = \frac{1}{2} E_0 \frac{k_C}{1-k_C}$. It follows that $\frac{\delta k_C}{k_C} = (1 - k_C)\frac{\delta q_l}{q_l}$ where δk_C is the change in k_C resulting from a change δq_l in q_l. This means there will be a shift in the position of the coherent edge at $\sim$240 MeV of approximately 0.07 MeV due to the estimated change to the inter-atomic plane separation. However, if d changes, the volume of the crystal and the orientations of the lattice planes relative to those of an undamaged part of the crystal will be affected. Referring to figure 8, the maximum shift in the rocking curves takes place over a distance of $\sim$0.5 mm on the crystal. The change of 4×10^{-4} in d will produce a change in the thickness of the diamond of $\sim$ 0.04 μm leading to an average angular change of $\sim$ 40 μrad in the orientation of the planes. This level of angular distortion of the lattice planes will produce a shift of $\sim$ 1.1 MeV in the position of the bremsstrahlung coherent edge at $\sim$ 240 MeV.

A shift in the coherent edge of about this value is observed experimentally for sample 6 and is illustrated in figure 11, which consists of four diagrams, each showing two bremsstrahlung spectra at two different points on the diamond. The coordinates of these points are shown on the top right corner of each diagram. Each pair of spectra has a common z co-ordinate, but x co-ordinates that are symmetrically placed with respect to the damage center. The spectra were taken using the same electron beam incident angle with respect to the diamond, and hence each spectrum should have the same edge position. However, from figures 11 (a), (b) and (c), a difference between the two bremsstrahlung peak positions of around 1 to 2 MeV is seen, which is close to the value estimated above. For figure 11 (d), where the two points are farthest from the damage centre, the peak position difference is much smaller. Comparing figures 10 and 11 which have the same co-ordinate system, we see the points selected in figure 11 are around the boundary of the region of maximum damage. From other coherent bremsstrahlung spectra measurements within the damaged region we also find the coherent edge positions do not show any significant variation and are located approximately mid-way

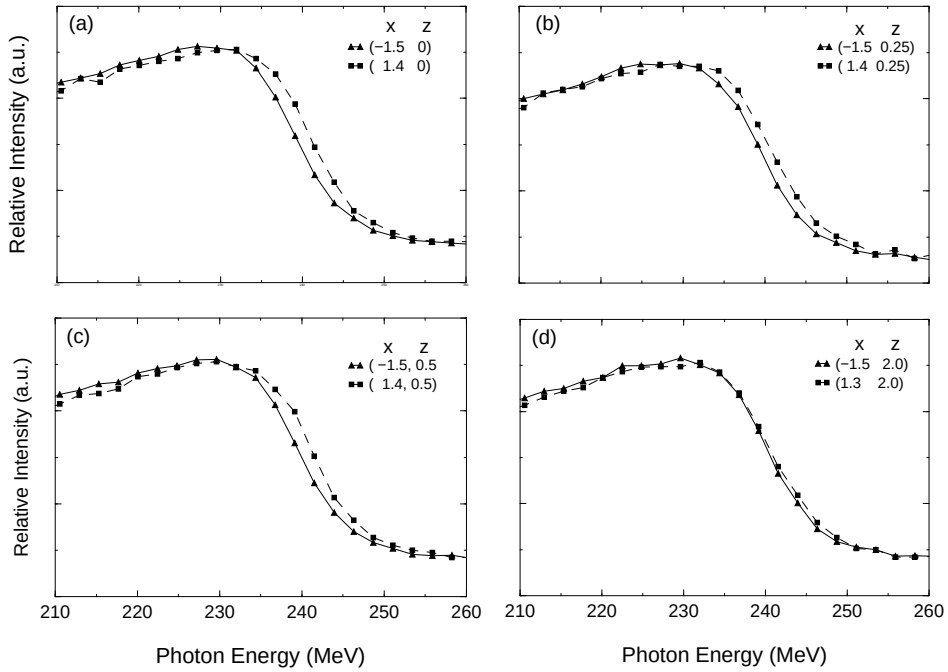

Fig. 11. Relative intensity $(I^{coh} + I^{incoh})/I^{incoh}$ of bremsstrahlung spectra for the sample 6 diamond at different positions. Referring to figure 7 the x-axis is horizontal and the z-axis vertical, with the origin at the damage centre.

between the pairs of curves shown in figures 11 (a), (b) and (c). These observations can be explained if it is assumed the diamond has a macro deformation in the form of a bulge which distorts the crystal lattice and extends over a region which is larger than the area of maximum damage. The lattice planes are distorted in opposite directions at the sides of the damage center, whereas close to the centre, the planes are approximately in their undamage orientation, but their separation has increased.

Volume changes have already been observed by other authors studying radiation effects (16). The polarized light analysis of radiation damaged diamond typically shows a stress pattern which has a uniform strain field with 4-fold symmetry which is like the stress caused by a large inclusion. Since this is exactly the form of the image shown in figure 7(b), this provides further evidence that sample 6 has a macro deformation.

To summarise our interpretation of the measurements shown in figure 8, we think there are two main effects which are interlinked. Firstly, there is a local increase in the disorder present in the diamond crystal lattice around the beam spot which leads to a broadening of the coherent edge, and secondly, a macro strain is induced in the diamond resulting in a small increase in the inter-atomic plane spacing.

We shall now consider some of the implications the preceding discussion has for higher electron beam energies. Since the characteristic angle for a higher electron beam energy is much smaller, the shape of the coherent edge is much more sensitive to the beam divergence, multiple scattering, and crystal dam-

age. For example for 12 GeV, the characteristic angle is about 42 μrad. Hence, if we use a beam divergence of 15 μrad, which will be an average value for the GlueX project, and have a 40 μm thick diamond which has an average plane projected r.m.s. multiple scattering angle of about 10 μrad, then if the crystal contribution changes from 10 μrad to 120 μrad - the values found due to radiation damage in sample 6 - the total angular spread will change from $\sim$20 μrad to $\sim$120 μrad. Referring to figure 3(b) an angular spread of 120 μrad would result in an r.m.s. spread in the upper edge energy of the coherent peaked at $E_\gamma \sim 8$ GeV of around 120 MeV. When the coherent photon spectrum is folded with the distribution of edge energies we find the width W of the coherent edge would have estimated values of 46 ± 6 MeV and 270 ± 36 MeV for undamaged and damaged parts of the crystal. The resulting smearing of the coherent bremsstrahlung peak from a damaged region would lead to a substantial decrease in the degree of linear polarisation, particularly if the photon beam is highly collimated (8).
For the GlueX experiment we now estimate how long it would take for this level of damage to occur. We assume the level of damage is proportional to the number of electrons passing through unit area of the diamond. The GlueX 12 GeV electron beam spot at the radiator is designed to have a transverse size of $\sim$1.7 mm $r.m.s.$ and a vertical size of $\sim$0.5 mm $r.m.s.$ Since the electron beam spot used for coherent bremsstrahlung production at Mainz has a diameter $\sim$0.1 mm $r.m.s.$ the area of the GlueX beam spot will be $\sim$84 times that of the beam spot at Mainz. If we assume the total estimated number of 10^{19} electrons through the Mainz diamond consisted of $\sim 5 \times 10^{17}$ electrons through 20 separate beam spots, then the number of $electrons/mm^2$ responsible for the level of radiation damage observed was $\sim 6.4 \times 10^{19}$ $electrons/mm^2$. Across the area of the GlueX beam spot this translates to a total of $\sim 4.2 \times 10^{19}$ electrons. If GlueX has a full intensity beam current of 3 μA the experiment could run for $\sim$1 month at full intensity before the diamond would experience radiation damage similar to that of the Mainz crystal. However, this level of radiation damage would be too high for GlueX, and it will be essential to monitor the number of the electrons $/mm^2$ passing through the crystal and limit the exposure of the diamond to the electron beam.

6 Conclusions.

In this paper we have considered how the angular spread of an electron beam passing through a diamond is affected by the divergence of the beam, the thickness of the crystal and the presence of defects in the lattice. Independently of the beam energy the optimum thickness for a diamond radiator is around 40 μm. We have demonstrated that the techniques of polarized light

analysis, X-ray topography and measuring X-ray rocking curves provide complementary information about the crystal lattice. ie: featureless polarised light and topographic images seem to correspond to narrow rocking curves and are typical of diamonds with few lattice defects. Furthermore, it is possible to obtain diamond specimens of very high quality from synthetic industrial diamonds.
We have also discussed the effects of the incident electron beam on coherent bremsstrahlung production. The following effects have been found for sample 6, the radiation damaged diamond.

(1) The atomic disorder resulting from defects caused by the incident electron beam does not have a significant effect on the general shape of a coherent bremsstrahlung spectrum, even though the corresponding rocking curve width is significantly broadened by radiation damage.
(2) The crystal imperfections cause the coherent edge width to become slightly broader.
(3) There is an induced strain leading to a small coherent bremsstrahlung edge shift across the region of strain. We conclude that this is caused by changes to the inter-atomic plane spacing which results in a small increase in the volume of the crystal.

For a 12 GeV electron beam, a thin high quality diamond crystal with a small mosaic spread is essential. In particular, for a 40 μm diamond, if the crystal contribution to σ_{total} changes by a factor of 12 from 10 to 120 μrad due to radiation damage, it is estimated the width of the coherent edge at 8 GeV will change by a factor of 6, from around 46 MeV to around 270 MeV. Since the resulting reduction in the degree of linear polarisation of collimated coherent bremsstrahlung photons would be significant, the level of damage from the electron beam should be closely monitored by noting if the width of the coherent edge increases.
At the beginning of the paper, we stated that one of our aims was to investigate if there was a simple and inexpensive assessment technique which could provide sufficient information to determine how well a diamond would perform as a radiator. Ideally, the hope would be that a featureless image from optical polaroid microscopy would be sufficient. Unfortunately, this is probably not the case as is demonstrated in figures 12 and 13. Figure 12 shows transmission topographs of 4 slices, each 100 μm thick, cut from a single synthetic diamond (which has not been discussed previously in the paper). The corresponding polarized light images are essentially the same as the topographs. The progression from (a) to (d) illustrates how the features in the topographs change with distance from the seed crystal. Figure 12(d), which is furthest from the seed, appears relatively featureless, but the rocking curve for 12(d), shown in figure 13, reveals a complex structure which extends across an angular range of $\sim$150 μrad, so that this diamond would be unsuitable for GlueX. On the other hand, the polarized light image shown in figure 4(a) is for one of

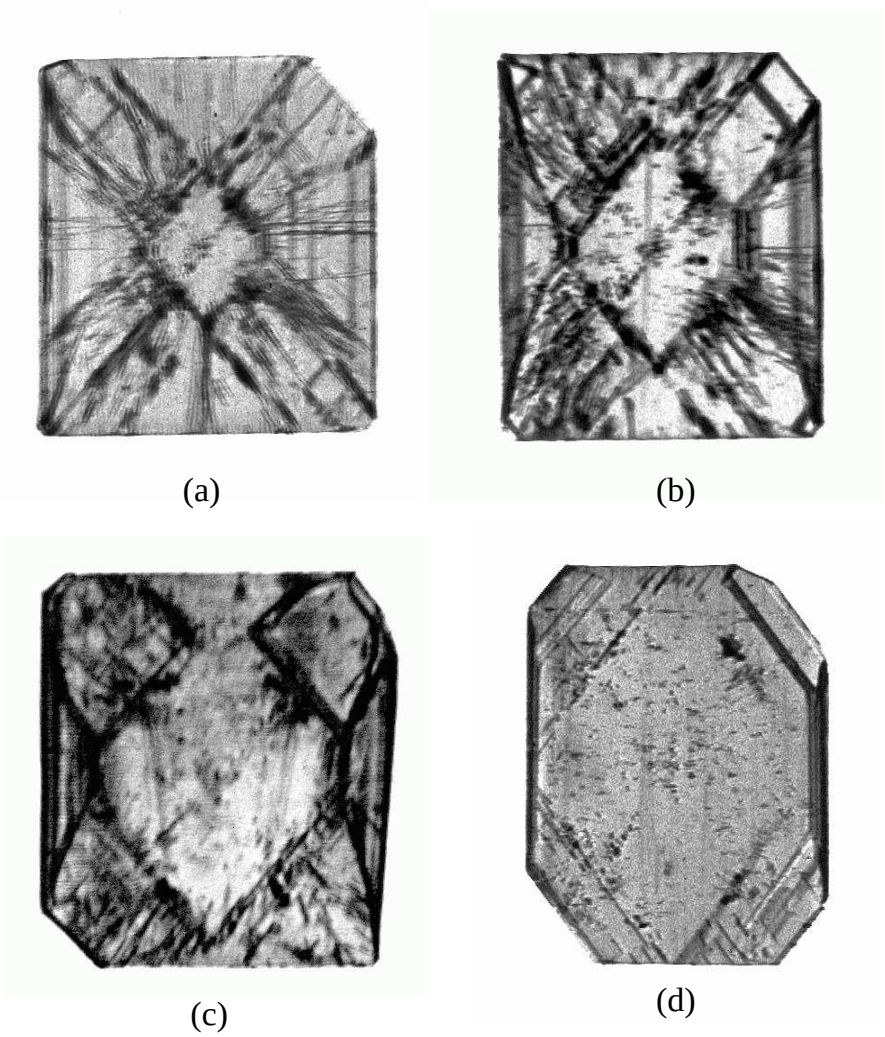

Fig. 12. Transmission topographs for four 100 μm sections cut from a single synthetic diamond

a set of 3 slices cut from another single synthetic diamond. All 3 slices have very similar polarized light images and transmission topographs and narrow rocking curves. Consequently, if it is possible to obtain several slices from the same synthetic diamond and they all have similar featureless polaroid images, then there is probably no need for an X-ray analysis. However, for a diamond on its own, irrespective of whether it is natural or synthetic, it would be sensible to carry out an X-ray analysis. Furthermore, since the quality of a diamond radiator being used in an experiment with linearly polarised photons will determine the degree of linear polarization of the photon flux, it would be inadvisable to use a radiator which had not received a thorough assessment. This is particularly important if beam energies greater than several GeV are being used.

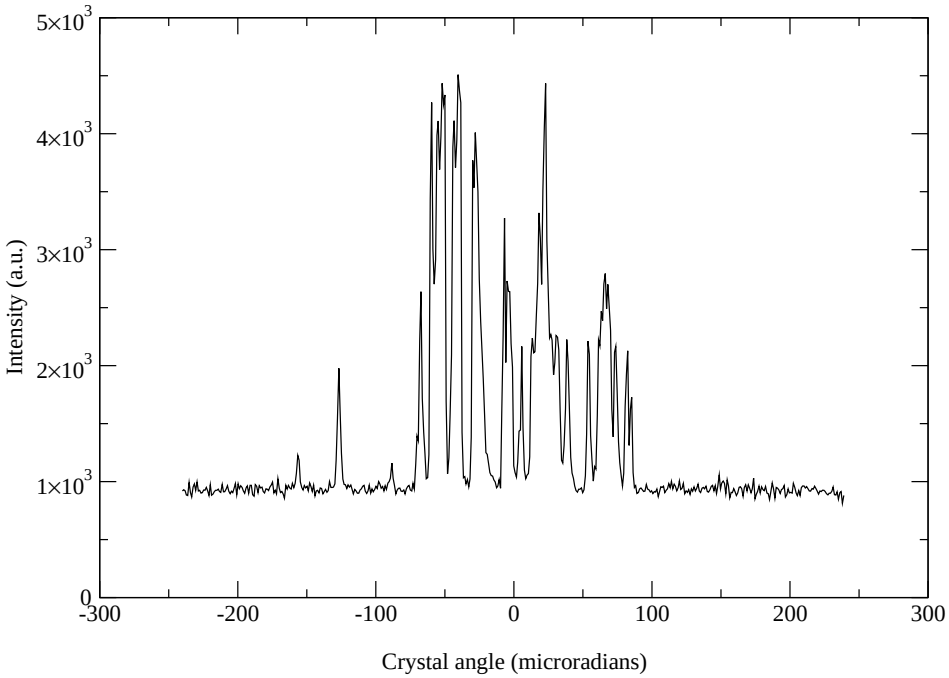

Fig. 13. Rocking curve for diamond section with topograph shown in fig 12(d)

The authors acknowledge support of this work by the Engineering and Physical Sciences Research Council and would also like to thank the Director of the Synchrotron Radiation Source at Daresbury and the Director of the Institüt für Kernphysik at Mainz University. They also acknowledge the help received from Element 6 for their expertise in polishing the diamond samples.

References

[1] D. Lohmann *et al.*, *NIM A* **343** (1994) 494.
[2] A. Natter, *A Coherent Bremsstrahlung Simulation Code*, Private communication, (2001).
[3] U. Timm, *Fortschritte der Physik* **17** (1969) 765.
[4] G. D. Palazzi, *Rev. Mod. Phys.* **49** (1968) 611.
[5] G. Davies, *Diamond*, Adam Hilger, (1984).
[6] I. Anthony *et al.*, *NIM A* **301** (1991) 301.
[7] S. J. Hall *et al.*, *NIM A* **368** (1996) 698.
[8] The Science of Quark Confinement and Gluonic Excitations. *GlueX/Hall D Design Report*, Version 4, Jefferson Laboratary (2002).
[9] F. Rambo *et al.*, *Phys. Rev. C*, **58** (1998) 489.
[10] L. Montanet et al., *Phys. Rev. D*, **50** (1994) 1173.
[11] B. W. Batterman and H. Cole, *Rev. Mod. Phys.*, **36**, (1964) 681,
[12] A. Authier, *Dynamical theory of X-ray diffraction*, Oxford University Press, Oxford, 2001
[13] C. G. Darwin, *Phil. Mag.*, **43** (1922) 800.

[14] K. Livingston, *An Alignment Technique for Diamonds used in Coherent Bremsstrahlung Experiments*, Private communication, (2002).

[15] J. L. Hubbell, Spectrum of thin Target Bremsstrahlung bounded by a forward circular Cone, *J. Appl. Phys.* , **30** (1959) 981.

[16] R. Kalish, A. Reznik, et al. *Nuclear Instruments and Methods B* ,**148** (1999) 626-633.